LA-UR- 09-00811

Approved for public release;
distribution is unlimited.

Title:	Terahertz Spectroscopy of Two-Dimensional Subwavelength Plasmonic Structures
Author(s):	A.K. Azad, H. Chen, A. Taylor, J.F. O'hara, J. Han, X. Lu, W. Zhang
Intended for:	SPIE Photonic West San Jose, CA 1/29/2009

Los Alamos
NATIONAL LABORATORY
EST.1943

Form 836 (7/06)

Terahertz spectroscopy of two-dimensional subwavelength plasmonic structures

Abul K. Azad, Hou-Tong Chen, Antoinette J. Taylor, and John F. O'Hara
Center for Integrated Nanotechnology, Los Alamos National Laboratory
Los Alamos, NM 87545
Jiaguang Han, Xinchao Lu, and Weili Zhang
School of Electrical and Computer Engineering, Oklahoma State University,
Stillwater, OK 74078
Email: aazad@lanl.gov, weili.zhang@okstate.edu

Abstract

The fascinating properties of plasmonic structures have had significant impact on the development of next generation ultracompact photonic and optoelectronic components. We study two-dimensional plasmonic structures functioning at terahertz frequencies. Resonant terahertz response due to surface plasmons and dipole localized surface plasmons were investigated by the state-of-the-art terahertz time domain spectroscopy (THz-TDS) using both transmission and reflection configurations. Extraordinary terahertz transmission was demonstrated through the subwavelength metallic hole arrays made from good conducting metals as well as poor metals. Metallic arrays made from Pb, generally a poor metal, and having optically thin thicknesses less than one-third of a skin depth also contributed in enhanced THz transmission. A direct transition of a surface plasmon resonance from a photonic crystal minimum was observed in a photo-doped semiconductor array. Electrical controls of the surface plasmon resonances by hybridization of the Schottkey diode between the metallic grating and the semiconductor substrate are investigated as a function of the applied reverse bias. In addition, we have demonstrated photo-induced creation and annihilation of surface plasmons with appropriate semiconductors at room temperature. According to the Fano model, the transmission properties are characterized by two essential contributions: resonant excitation of surface plasmons and nonresonant direct transmission. Such plasmonic structures may find fascinating applications in terahertz imaging, biomedical sensing, subwavelength terahertz spectroscopy, tunable filters, and integrated terahertz devices.

1 Introduction

In recent years, two-dimensional (2D) metallic arrays of subwavelength holes, which enable extraordinary transmission of electromagnetic waves via excitation of surface plasmon resonance, have been studied with a great interest because of their possible applications in integrated nano and micro-photonics. Understanding the physical origin of resonant properties in such plasmonic structures has been of special interest because of their possible breakthrough applications in semiconductor nanofabrication, microscopy, display technology, tunable filters, and bio-chemical sensing[1-3]. Surface plasmons (SPs) are collective excitations for quantized oscillations of electrons[4]. The resonant interaction between electron-charged oscillations near the surface of metal and the electromagnetic field creates SPs and results in rather unique properties[5]. Recent advance in extraordinary transmission of light has demonstrated when light passed through periodic subwavelength holes perforated in a metallic film and the resulted higher-than-unity transmission was primarily attributed to resonant excitation of SPs[1,3]. Light was coupled into the holes in the form of SPs which were squeezed through the holes and then converted back into light on the far side of the holes.

In the terahertz regime, SPs have recently attracted much attention and become an attractive new area[6-13]. Due to a drastic increase in the value of dielectric function $\varepsilon_m = \varepsilon_{rm} + i\varepsilon_{im}$, most metals become highly conductive at terahertz frequencies. This has resulted in discrepancies in SP-enhanced transmission of terahertz radiation with that in the visible spectral regime. Experimental results on transmission properties of light in metallic structures have indicated that SP-enhanced transmission is normally achieved in metals with large ratio of the real to the imaginary dielectric constant, $-\varepsilon_{rm}/\varepsilon_{im} >> 1$[14,15]. In the terahertz regime, however, this ratio becomes $-\varepsilon_{rm}/\varepsilon_{im} < 1$ for non-transition metals, such as Ag, Au, Cu, and Al[16]. This was considered as a limitation to realize resonant excitation of terahertz SPs in the

periodic subwavelength structures. The recent studies, however, have demonstrated that an appropriate surface corrugation provided by the subwavelength structures could facilitate the resonant excitation of SPs even with $-\varepsilon_{rm}/\varepsilon_{im} < 1$[17]. SP-enhanced terahertz transmission has been experimentally observed in subwavelength hole arrays patterned in metal films made from both good and generally poor metals[18,19]. In addition to metals, semiconductors with high density of free carriers exhibit metallic properties by having a negative real part of dielectric function ($\varepsilon_{rm} < 0$), and thus can be used as alternate metallic media to support SPs at terahertz frequencies. As a result, enhanced terahertz transmission was demonstrated in microstructured hole arrays made from both intrinsically doped and photo-doped semiconductors[7,20-24]. The advantage of semiconductors is that their dielectric function can be modified by varying doping concentration, temperature, or optical excitation. This in turn enables tuning and switching of SPs. Such semiconductor plasmonic arrays may find applications in all solid state terahertz optoelectronic devices, such as high-throughput, high resolution filters, and focusing elements for terahertz imaging system.

In this article, we present our recent work on resonant terahertz transmission in lithographically fabricated 2D metal and semiconductor arrays of subwavelength holes. The presentation is organized as follows: in section II, we describe experimental methods employed in these studies, including terahertz time-domain spectroscopy and optical pump-terahertz probe spectroscopy. In section III, the lithographic fabrication processes of the plasmonic arrays are presented. In section IV, we review resonant terahertz transmission in metal arrays of subwavelength holes. The interesting properties of plasmonic structures made from semiconductors are introduced in section V. We present the switching of the SP resonances in section VI by employing electrical and optical techniques. Finally, section VII gives a conclusive discussion.

2 Experimental Methods

2.1 Terahertz time-domain spectroscopy

Broad-band photoconductive switch-based terahertz time-domain spectroscopy (THz-TDS) transmission measurements were employed to study resonant properties of the 2D intrinsic plasmonic arrays. Figure 1 sows the schematic diagram of a photoconductive antenna based THz-TDS system which comprised of a GaAs transmitter, a silicon-on-sapphire (SOS) receiver, and four parabolic mirrors, aligned in an 8-F confocal geometry[19]. A self-mode-locked Ti:sapphire laser capable of generating 88-MHz, 800-nm, and 26-fs ultrafast optical pulses was used to gate the photoconductive switches, with 10-mW average power on each side. This 8-F confocal system not only ensured an excellent beam coupling between the transmitter and receiver but also compressed the terahertz beam to a frequency independent diameter of 3.5 mm. The THz-TDS system has a useful bandwidth of 0.1 to 4.5 THz (3 mm – 67 μm) and a signal-to-noise ratio (S/N) of > 15,000:1.

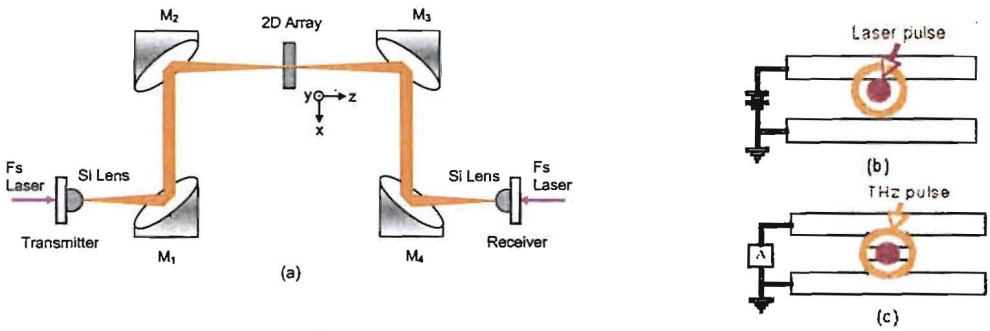

Fig. 1 Schematic diagram of the terahertz time-domain spectroscopy system: (a) the 8F confocal system; (b) GaAs transmitter; (c) silicon on sapphire receiver.

In the transmission measurements, the array was placed midway between the parabolic mirrors, M_2 and M_3, at the waist of the terahertz beam. The terahertz radiation transmitted through the array at normal incidence with a *P*-polarized electric field. A blank slab identical to the array substrate was used as a reference. The transmitted electric field of the terahertz pulses through the sample and reference were recorded in time domain and then Fourier-transformed into

frequency-domain amplitude spectra as $E_a(\omega)$ and $E_r(\omega)$, respectively. The absolute amplitude transmission of the array was defined as $|\tilde{t}(\omega)| = |E_a(\omega)/E_r(\omega)|$ and the corresponding phase change was obtained through the relation, $\phi(\omega) = \arg[t(\omega)]$.

2.2 Optical pump-terahertz probe spectroscopy

Optical pump-terahertz probe characterization was used to investigate resonant properties of the non-intrinsic plasmonic arrays of subwavelength holes, such as the photo-doped semiconductor samples[23]. The terahertz pulses were generated from a 2 mm-thick ZnTe crystals by optical rectification and were detected by use of electro-optical sampling in a 1-mm-thick ZnTe crystal[25]. A femtosecond regenerative Ti:sapphire amplifier, capable of generating 3.2-mJ, 50-fs intense laser pulses at a repetitions rate of 1 kHz, was used as the optical source for terahertz pulse generation, detection, and photo-doping of the semiconductor arrays. The generated terahertz pulses were guided towards the detector by four parabolic mirrors in a confocal geometry. The terahertz focal spot size between the two inner parabolic mirrors was 2 mm.

3 Sample fabrications

We fabricated subwavelength plasmonic arrays using conventional photolithography and thermal metallization processing. Metallic hole arrays were fabricated on high quality silicon (0.64-mm-thick, p-type resistivity ρ = 20 Ω cm) and on semi-insulating GaAs substrstes. The photolithography processing included spin application of photoresist adhesive promoter (HMDS, Microchem), spin coating of positive photoresist (S-1813, Shipley), convection oven bakes, contact mode exposure, and resist development (2401 developer, Microchem). The patterned wafer was then thermally evaporated (BOC-306) with a layer of metal films, such as Al, Ag, and Pb. A follow up process was acetone lift-off to reveal the metal patterns of subwavelength hole arrays[19]. A high resolution optical image of a square array of 100 mm × 80 mm rectangular holes of a periodicity of 160 mm is illustrated in Fig. 2(a). The freestanding arrays were fabricated from 30-50 μm-thick silicon wafers. The fabrication processes have included conventional photolithography and reactive ion etching (RIE) processes. The wafer was first spin-coated with SU-8 2025 photoresist (Microchem) and exposed with a UV light source while under the mask[21]. After development, the RIE process has created through-holes on the bare silicon while the rest of the area of the wafer was still protected with photoresist. A mixed gas flow of 12.5-sccm SF_6 and 1.5-sccm O_2 driven under a RF power of 400 W delivered an etching rate of 5 μm/min for silicon. Figure 2(b) shows a scanning electron microscopic (SEM) image of a freestanding array of elliptical holes with a periodicity of 160 μm and dimensions of 75 μm along the major axis (y) and 45 μm along the minor axis (x).

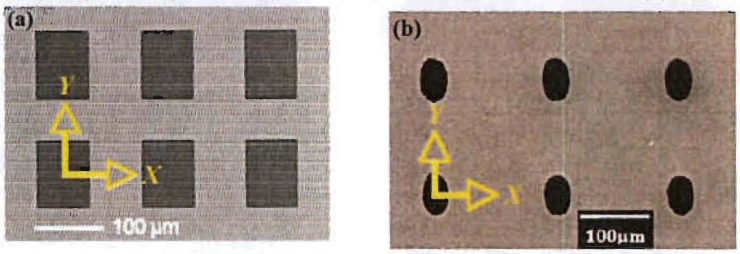

Fig. 2. Images of plasmonic arrays of subwavelength holes: (a) microscopic image of the metal array on silicon; (b) SEM image of the free standing array.

4 Resonant enhancement of terahertz transmission in metal arrays

In this section, we present our recent work on resonant terahertz transmission in both optically thick and optically thin 2D metal arrays of subwavelength holes. At the primary SP [±1,0] mode, amplitude transmission efficiency of up to nine tenths of the maximum resonant transmission was achieved when the thickness of the metallic array was only one third of the skin depth[6,18]. By use of highly reproducible subwavelength arrays we have demonstrated the effect of dielectric function of metals on transmission properties of terahertz radiation[19]. We have also shown that the enhanced terahertz transmission in the 2D arrays of subwavelength holes is resulted from contributions of both SPs and nonresonant transmission[26].

4.1 Resonant excitation of terahertz SPs in optically thick metal arrays

In the terahertz regime, THz-TDS measurements have revealed enhanced amplitude transmission and a sharp phase peak in 2D optically thick arrays of metal holes[6]. Correspondingly, the measured transmission magnitude has the shape of the derivative of this peak, which is consistent with the Kramers–Kronig relations. In addition, we found that the hole shape of the thin metallic films had a significant effect on the transmission magnitude and the corresponding phase change of the terahertz radiation. Each array was a lithographically fabricated 520-nm-thick aluminum film deposited on silicon substrate. To investigate the hole shape effect, two array samples were prepared. Sample A is a square array of 80 μm (x axis) × 100 μm (y axis) rectangular holes as shown in Fig. 2(a), while sample B is a square array of 100-μm-diameter circular holes. The periodicity of these arrays is L = 160 μm in both 2D directions.

The extracted amplitude transmission and the corresponding phase change are shown in Figs. 3(a) and 3(b), respectively. Several well-defined resonant features were observed and essentially attributed to resonant excitation of SPs at terahertz frequencies. In particular, the sharp resonance near 0.5 THz exhibits 2.26 and 1.45 power transmission efficiency for samples A and B, respectively, when normalized to the area occupied by the holes, as referred to as higher-than-unity extraordinary transmission[1].

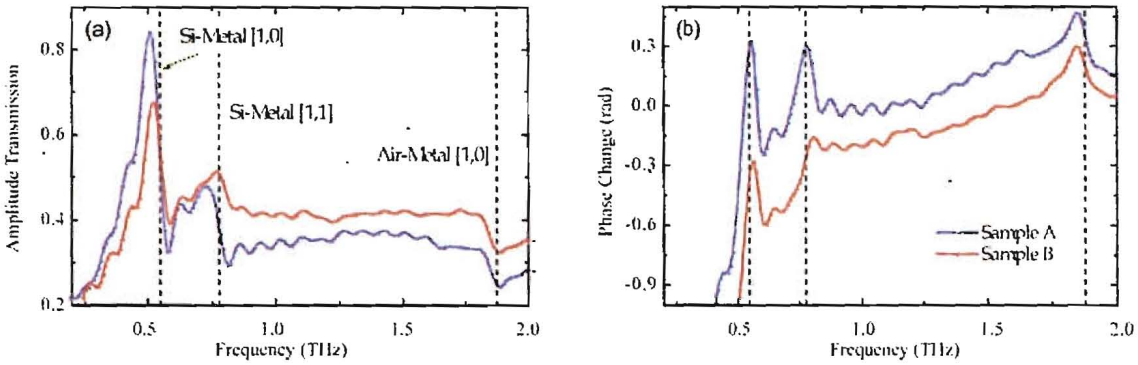

Fig. 3. (color online) (a) Measured frequency-dependent amplitude transmissions. (b) Corresponding comparative phase change in radians for Sample A, 80 mm ×100 mm rectangular hole arrays and Sample B, 100 mm diameter circular hole arrays. In (a), the spectrum of Sample B is lifted by 0.1 and in (b), the phase change of Sample B is lowed by 0.1 for clarification. The dashed lines indicate the SP resonance frequencies.

In a metal array, SPs can be resonantly excited at the metal-dielectric interfaces following momentum conservation[4,27], $\mathbf{k_{sp}} = \mathbf{k}_{\parallel} + \mathbf{G_{mn}}$, where $\mathbf{k_{sp}}$ is the wave vector of SPs, $\mathbf{k}_{\parallel}$ is the in-plane wave vector, $\mathbf{G_{mn}}$ is the reciprocal lattice vectors, m and n are integers of the SP modes. In a 2D array of subwavelength holes, the resonant frequencies of SPs at the metal-dielectric interface can be described through the dispersion relation at normal incidence as[4,27],

$$\omega_{sp}^{m,n} = cG_{mn}\left(\frac{\varepsilon_d \varepsilon_m}{\varepsilon_d + \varepsilon_m}\right)^{-1/2}, \qquad (1)$$

where ε_m and ε_d denote the dielectric function of metal and the adjacent dielectric medium, respectively, $G_{mn} = (2\pi/L)(m^2 + n^2)^{1/2}$ is the grating momentum wave vector for the 2D square hole arrays, L is the periodicity of the array, c is the speed of light in vacuum.

In the terahertz regime, the dielectric constant of metals is several orders higher than that of dielectric media. For example, $\varepsilon_m = -1.12\times10^5 + 1.45\times10^6 i$ for aluminum at 0.55 THz, while $\varepsilon_d = 11.68$ and $\varepsilon_d = 1$ for silicon and air, respectively. Thus, the SP modes excited in the array can be approximately given as[4,6,27] $\omega_{SP}^{m,n} \cong cG_{mn}\varepsilon_d^{-1/2}$. The observed sharp phase peaks centered at the SP resonance modes are indicated by the vertical dashed lines: the metal-Si modes at 0.55 [±1,0] and 0.78 [±1,±1] THz; the metal-air mode [±1,0] at 1.88 THz. Besides samples A and B, a set of arrays with

rectangular, square, and circular holes has been measured. We observed that with the same fundamental period the hole shape and dimensions could appreciably modify the strengths and shapes of the transmission and the phase change peaks due to the polarization dependent coupling of SPs.

4.2 Evolution of terahertz SP resonance in optically thin metal arrays

Resonant excitation of SPs has been widely studied in optically thick 2D hole arrays in a broad spectral range. It is interesting, however, whether SPs can be excited in optically thin metallic arrays of sub-skin-depth thicknesses. Here, we demonstrate resonant terahertz transmission through subwavelength hole arrays patterned on metallic films with thicknesses less than a skin depth. Our experimental results have revealed a critical array thickness, above which the SP resonance begins to establish[18]. The maximum amplitude transmission was achieved when the thickness of metal film approaches a skin depth. However, enhanced terahertz transmission of up to nine tenths of the maximum transmission was realized at a film thickness comparable to the skin depth at wavelengths of light, only one third of the skin depth at the metal-silicon [±1,0] SP mode, 0.55 THz.

We have processed a set of metallic arrays of subwavelength rectangular holes from Pb film deposited on the silicon wafer[18]. The rectangular holes have physical dimensions of 100 μm × 80 μm with a periodicity of 160 μm. Pb was chosen as the constituent metal of the arrays mainly because of two reasons. First, extraordinary terahertz transmission in Pb subwavelength hole arrays has been demonstrated with an amplitude efficiency of up to 82% at 0.55 THz, which is close to the performance of arrays made from good electrical conductors such as Ag, Al, and Au[16,19]. Second, the skin depth of Pb at 0.55 THz is 320 nm, nearly three times of those of Ag and Al. It thus provided a large dynamic range to characterize the evolution of SP resonance at sub-skin-depth thicknesses.

The value of skin depth of electromagnetic waves in metal is determined by the penetration distance at which the electric field falls to $1/e$. The SPs, which propagate along metal-dielectric interface, decay exponentially in both media. At terahertz frequencies, the complex wave vector inside the metal perpendicular to the interface (k_z) and the corresponding skin depth (δ) are approximately given as[6,15,18],

$$k_z = \frac{\omega}{c}\varepsilon_m^{1/2}, \qquad (2) \qquad \text{and} \qquad \delta = \frac{1}{\mathrm{Im}(k_z)} = \frac{c}{\omega}\frac{1}{\mathrm{Im}(\varepsilon_m^{1/2})} = \left(\frac{2}{\omega\mu_0\sigma_{dc}}\right)^{1/2} \qquad (3)$$

where ω is the angular frequency where μ_0 is the vacuum permeability and σ_{dc} is the d.c. conductivity of metal. Based on this relation, frequency dependent skin depths of various metals are plotted in the terahertz regime in Fig. 4(a). As can be seen, the skin depths for Pb, Al, and Ag at 0.55 THz, the primary SP [±1, 0] resonance, are estimated to be 320, 110, and 83 nm, respectively.

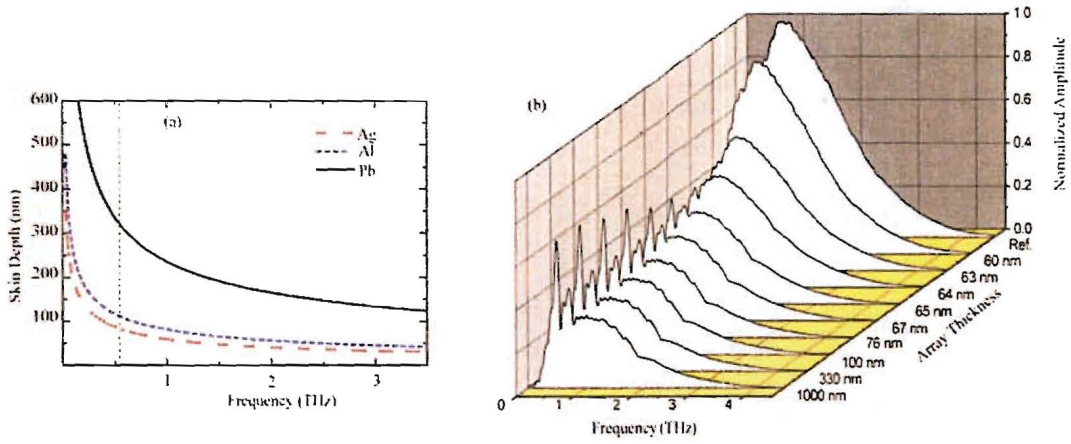

Fig. 4. (a) Calculated frequency dependent skin depth of metals at THz frequencies. (b) Measured THz spectra of reference and metal gratings having different thickness.

We prepared Pb arrays with various thicknesses ranging from 60 to 1000 nm. Measured THz spectra through the reference and arrays of different thickness are shown in Fig. 4(b). During measurements THz polarization was along the

minor axis of the holes at normal incidence. When the array film is thin, the spectrum showed no resonance but similar features of the reference spectrum with attenuation. At 64 nm, which was observed as a critical thickness for the Pb array, the SP resonance excited at the Pb-Si interface appeared in the spectrum. Above this critical thickness, the resonance peak is enhanced with thicker array film.

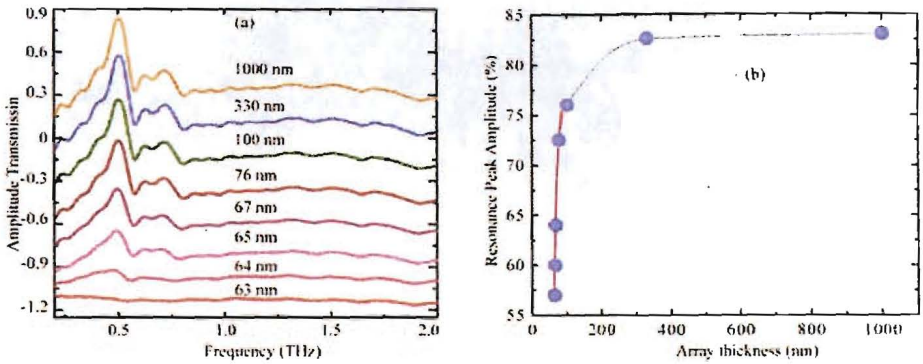

Fig. 5. (a) Measured amplitude transmission of the Pb arrays with different thicknesses. The curves are vertically displaced for clarity. Measured peak amplitude of the [±1, 0] SP mode at 0.55 THz as a function of the Pb thickness (dots), connected by a dotted curve to guide the eye. The solid curve is an exponential fit for the region of array thicknesses below 100 nm.

In Fig. 5(a), evolution of SP resonance as a function of array film thickness is depicted in the amplitude transmission spectra of various arrays. It clearly reveals two regions of thickness dependence. Below the critical thickness, 64 nm, the frequency-dependent transmission is nearly flat, showing no resonance peak. Above the critical thickness, a resonance at 0.55 THz appears in the transmission, whose amplitude increases with array thickness while the background transmission is reduced at the mean time. This resonance is attributed to the excitation of SPs at the Pb-Si interface. Immediately above the critical thickness, the resonance amplitude is very sensitive to the thickness of arrays. The dependence of peak transmission on array thickness above the critical thickness is shown in Fig. 5(b). The amplitude transmission efficiency increases exponentially when the array thickness is below 100 nm. It then saturates gradually and approaches the maximum at one skin depth[18]. It is worth noting that a transmission efficiency as high as 76% was achieved at array thickness of 100 nm, only one third of skin depth. For comparison, we have fabricated two additional arrays of same structure but made from Ag and Al of one third of skin depth. The measured transmission efficiencies are all above nine tenths of their maximum amplitude transmission. This finding may extensively reduce the metal thickness of plasmonic components for applications in photonic, optoelectronic, and sensing devices.

4.3 Effect of dielectric function of metals on resonant terahertz transmission

The dielectric function of constituent metals was found to play an essential role in the extraordinary transmission of light in 2D subwavelength hole arrays. Owing to different ratio of the real to imaginary dielectric function, $-\varepsilon_{rm}/\varepsilon_{im}$, transmission properties of light showed a large difference in the arrays made from Ag, Au, and Cr[1,14,15]. The SP-enhanced transmission efficiency of light was increased with higher ratio $-\varepsilon_{rm}/\varepsilon_{im}$, for example, the transmission efficiency of Ag arrays was several times higher than that of Ni arrays of the same structure[15]. At terahertz frequencies, however, the values of dielectric function of metals are several orders of magnitude higher than those at visible frequencies. The dielectric function of metals may influence the extraordinary terahertz transmission differently in subwavelength structures than that at visible frequencies.

To explore dielectric function related terahertz transmission properties of metal arrays at different resonance frequencies, two types of array samples were lithographically fabricated: array-on-silicon samples with patterned optically thick metal film on blank silicon substrate for the metal-silicon [±1,0] mode at 0.55 THz[6,19] and freestanding metallic arrays for the metal-air [±1,0] mode at 1.60 THz[19,21]. Our THz-TDS measurements have shown that the resonant

terahertz transmission was increased with the higher ratio $-\varepsilon_{rm}/\varepsilon_{im}$ for metals with dielectric function following the Drude model. This result is consistent with the observation at optical frequencies[14,15].

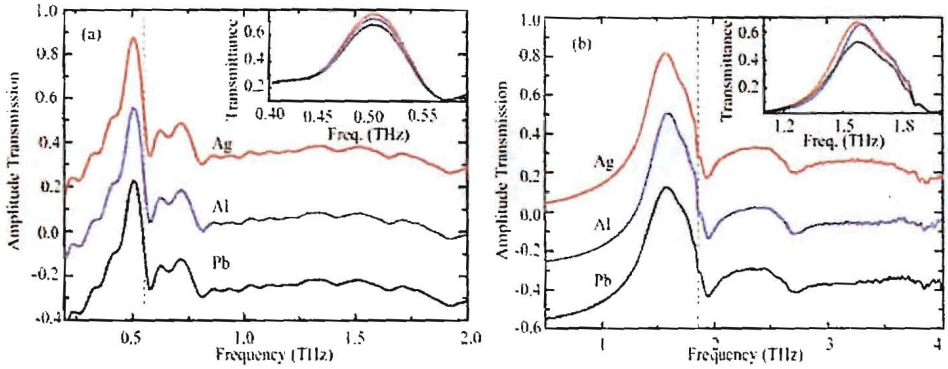

Fig. 6. Measured amplitude transmission: (a) array-on-silicon and (b) free-standing samples made from Ag, Al, and Pb. For clarity, the spectra of Al and Pb arrays are moved. The vertical dashed line indicates the calculated [±1, 0] metal-Si and metal-air SP. The inset shows the corresponding transmittance.

The dielectric function of the non-transition metals such as Ag, Al, and Pb can be well described by the Drude model[16], $\varepsilon_m(\omega) = \varepsilon_\infty - \omega_p^2/(\omega^2 + i\omega\Gamma)$, where $\omega_p/2\pi$ is the plasma frequency, $\Gamma/2\pi$ is the carrier damping frequency, and ε_∞ is the high frequency dielectric constant. Based on the experimentally determined parameters given in Ref. 22 we calculated the dielectric constant at THz frequencies and found that the absolute values of both the real and the imaginary parts of dielectric function are several orders of magnitude higher than that at visible frequencies.

At 0.55 THz, the ratios $-\varepsilon_{rm}/\varepsilon_{im}$ for Ag, Al, and Pb are 0.12, 0.03, and 0.01, respectively, indicating that Ag is still a better metal than others, and was expected to show resonance with higher amplitude transmission[15]. Practically, as shown in Fig. 6 (a), the Ag array indeed showed the highest amplitude transmission 87%, while the Al and Pb arrays followed after with small attenuation, giving 85.5% and 82%, respectively. Even though the amplitude transmission of these arrays revealed small differences, it indeed increased with higher ratio $-\varepsilon_{rm}/\varepsilon_{im}$. This showed good consistency with those observed at visible frequencies[14,15]. Compared to excellent metals, Pb is generally considered as a poor electrical conductor. However, the drastic increase in dielectric constant enables Pb to behave as a better metal towards the establishment of SP-enhanced transmission at terahertz frequencies. In Fig. 6(b), the measured peak transmission at the SP [±1,0] resonance 1.60 THz for Ag, Al, and Pb are 82%, 81%, and 72.5%, respectively, showing similar properties as observed at the SP [±1,0] metal-Si resonance 0.55 THz. The difference in amplitude transmission for arrays made from these metals was arisen from the difference in effective propagation length of SPs.

4.4 Coupling between SPs and nonresonant transmission

So far, SPs excited at the surface of 2D hole arrays have been considered as a dominant mechanism in extraordinary transmission of electromagnetic waves[1,4]. The recent studies, however, have revealed that besides SPs, localized waveguide resonances or localized modes also make contributions to the extraordinary transmission of light in periodic subwavelength holes[28,29]. To better understand the transmission enhancement mechanism in the terahertz regime, we have studied hole width-dependent terahertz transmission. A characteristic evolution, including well-regulated change in transmittance, linewidth broadening, and blueshift of peak transmission frequencies with respect to hole width were experimentally observed[26]. Based on numerical analysis by the Fano model, we found that terahertz transmission in the 2D hole arrays were associated with two types of contributions, resonant excitation of SPs and nonresonant transmission (or non-SP transmission). The localized effects, as either localized modes or localized waveguide resonances[28,29], also contributed substantially to enhanced terahertz transmission.

In sample preparation, a set of 2D hexagonal arrays of rectangular subwavelength holes are lithographically

fabricated with a 180-nm-thick Al film onto a silicon substrate[26]. Each sample, with dimensions of 15 × 15 mm^2, has holes of a fixed length 120 μm and various widths from 40 to 140 μm with a 20-μm interval, and has a constant periodicity of 160 μm. Figure 7(a) illustrates the frequency-dependent absolute transmittance and the corresponding phase change for an array with hole dimensions of 120 × 40 μm^2. At normal incidence, the resonant frequency can be approximately given by equation (1) with the grating momentum wave vector, $G_{mn} = 4\pi\left(m^2 + n^2 + mn\right)^{1/2}/\sqrt{3}L$ for the 2D hexagonal hole arrays. The calculated fundamental SP [±1,0] resonance of hexagonal arrays at the Al-Si interface was around 0.63 THz, which was higher than the measured transmission peak 0.49 THz due to the fact that the latter was a result of both resonant and nonresonant contributions[30].

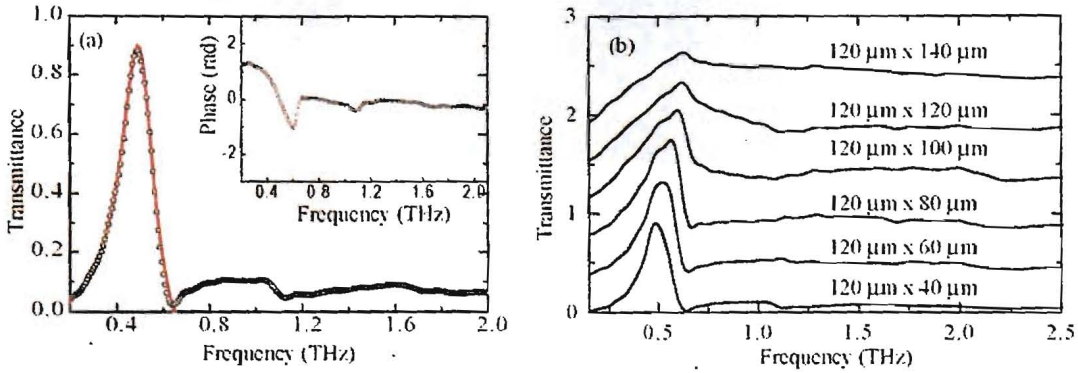

Fig. 7. (a) Measured (open circles) and the Fano fit (solid curve) of frequency-dependent transmittance. The fitting parameters are: q_v = 26.5 ± 0.2, $\omega_v/2\pi$ = 0.49 ± 0.05 THz, $\Gamma_v/2\pi$ = 0.16 ± 0.01 THz, and T_b = (1.28 ± 0.1) ×10^{-3} for the [±1,0] mode. Inset: corresponding data of phase change. (b) Measured frequency dependent absolute transmittance of the hole arrays with fixed hole length of 120 μm and various hole widths. The curves are vertically displaced for clarity.

The experimental transmittance was further analyzed by the Fano model, in which the transmission line shape of the arrays was considered as a result of two scattering processes: one refers to the continuum direct scattering state as non-resonant transmission, and the other is the discrete resonant state as SPs[23,30]. For an isolated resonance, the Fano model can be written as

$$T_{fano}(\omega) = \left|\tilde{t}(\omega)\right|^2 = T_a + T_b \frac{(\varepsilon_v + q_v)^2}{1 + \varepsilon_v^2}, \qquad (4)$$

where $\varepsilon_v = (\omega - \omega_v)/(\Gamma_v/2)$, T_a is a slowly varying transmittance, and $|T_b|$ is a coefficient that describes the contribution of a zero-order continuum state coupled to the discrete resonant state. The resonant state is characterized by the resonance frequency ω_v, the linewidth Γ_v, and the Breit-Wigner-Fano coupling coefficient q_v. The Fano model provided a consistent fit to the measured transmittance as shown in Figure 7(a) (solid line), with a peak transmission at $\omega_v/2\pi$ = 0.49 THz and a linewidth $\Gamma_v/2\pi$ = 0.16 THz.

To understand the coupling between SPs and nonresonant transmission, we have studied a set of arrays with various hole widths from 40 to 140 μm. The measured transmittance revealed a hole width dependent evolution, as shown in Figure 7(b). An optimal hole width exists, here was 80 μm, with which maximizes the peak absolute transmittance. However, there is a monotonic change in the resonance frequency and the linewidth which is mainly due to the coupling between SPs and nonresonant tranmission. We have calculated coupling strength between the SP mode and nonresonant transmission for arrays with different hole widths at normal incidence (explained else where[26]). With increasing hole width the coupling strength shows monotonic change; it is enhanced from $|\chi|^2 = 1.22 \times 10^{-3}$ at 40 μm to $|\chi|^2 = 6.21 \times 10^{-3}$ at 140 μm. The increase in hole width, that corresponded to reduced aspect ratio of holes and lower filling fraction of metal, not only led to increased direct transmission through the holes, but also enhanced the coupling between SPs and non-resonant transmission. This in turn gave rise to an increased damping of SPs and thus the linewidth broadened and shifted to higher frequencies towards the peak of nonresonant transmission[23,28,30]. For arrays with filling fraction of metal

less than 80%, direct transmission contributed substantially to nonresonant transmission and caused a monotonic decline in normalized transition efficiency.

5 Resonant terahertz transmission in semiconductor arrays

In this section, we present transmission properties of terahertz radiation in semiconductor plasmonic arrays made from both intrinsically doped and photo-doped silicon thin slabs. An array of elliptical holes made from highly n-doped silicon film has enabled a 175% transmittance when it was normalized to the areas occupied by the holes[21]. More interestingly, in a similar array made from lightly doped silicon, a characteristic evolution of a terahertz SP resonance was observed under variable optical excitations[23]. The SP resonance was developed from an out-of-plane photonics crystal resonance when the real part of dielectric function of the array was switched from positive to negative due to increased photogenerated free carriers.

5.1 Resonant terahertz transmission in highly-doped silicon arrays

We investigated resonant terahertz transmission of an array of subwavelength holes patterned on ultrathin, highly doped silicon. The zero-order transmission spectra exhibited well-defined maxima and minima, as attributed to the resonant excitation of SPs and Wood's anomaly, respectively[4,31]. Transmission anisotropy was investigated in terms of orientation of the elliptical hole array. It was observed that the transmission increased significantly when the major axis of the elliptical hole was perpendicular to the polarization of the terahertz radiation.

The silicon array, as shown in Fig. 2(b), was processed from a commercially available n-type, 50-μm-thick silicon wafer with a resistivity of $2\times10^{-3}\Omega$ cm. The carrier density and the thickness of the doped silicon were chosen to ensure that no terahertz transmission was observed through the unstructured silicon slab. In fact, the corresponding amplitude absorption length was less than 1 μm at 1 THz. At 1.0 THz, with given n-type carrier density, $3\times10^{19}\text{cm}^{-3}$ and a corresponding electron mobility, 120 cm^2/Vs, the real and imaginary dielectric constants are $\varepsilon_{rm}=-103$ and $\varepsilon_{m2}=1020$, respectively. The ratio $-\varepsilon_{rm}/\varepsilon_{im}=0.10$ is compatible with that in Al[6], indicating the possibility of resonant excitation of SPs in the silicon array at terahertz frequencies.

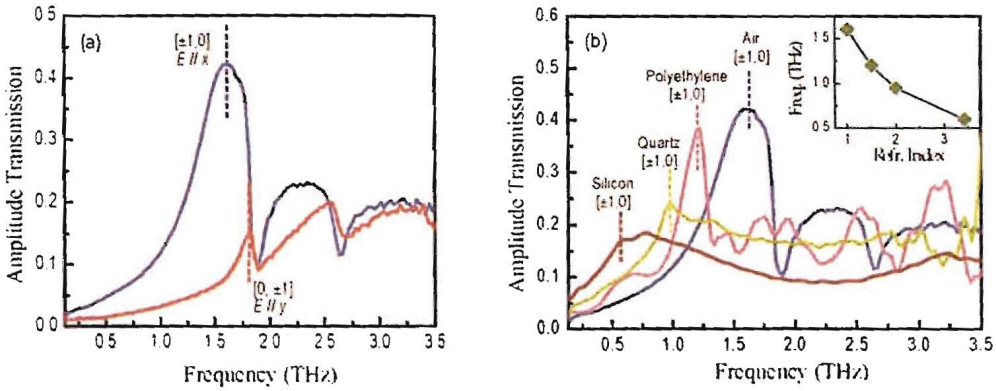

Fig. 8. (a) Amplitude transmission through silicon hole array. (b) Comparison of transmission spectra for different dielectric-array interfaces. The dashed lines represent the [±1, 0] resonance peaks. Inset: measured resonance frequencies of the [±1, 0] SP modes as a function of the surrounding refractive index.

The frequency dependent amplitude transmission spectra for both array orientations, $E||x$ and $E||y$, are shown in Figure 8(a). For the case of $E||x$, the transmission spectrum showed a pronounced peak at 1.6 THz, well below the cutoff, which was 2.0 THz as determined by the 75-μm-sized holes[7,20]. The peak of the transmission magnitude was due to the resonance of SPs and can be attributed to the [±1, 0] SP mode as indicated by a dashed line. We observed a 42% amplitude transmission for the [±1, 0] mode at the silicon-air interface, which led to a power transmission efficiency of 175% when normalized by the voided areas of the holes. In contrast, the resonance peak of the SP [0, ±1] mode for the

$E||y$ orientation was located at 1.8 THz and showed an amplitude transmission efficiency of 16%.

The minima shown in Fig. 8(a) were identified as the result of Wood's anomaly observed in diffraction grating structures[31]. Wood's anomaly minima occur when a diffracted order becomes tangent to the plane of grating. For a square lattice and normal incidence the wavelengths of Wood's anomaly minima can be approximately given by[32] $\omega_{Wood}^{m,n} = cG_{mn}\varepsilon_d^{-1/2}$. The two calculated Wood's anomaly minima are located at 1.875 [±1, 0] or [0, ±1] and 2.652 [±1, ±1] THz, respectively, for the doped silicon-air interface. When the surrounding dielectric constant $\varepsilon_d << \varepsilon_m$, the resonant frequency for SPs given in Eq. (2) may overlap with the frequency of Wood's anomaly minima.

The dependence of SP-assisted transmission properties on the dielectric function of surrounding media were investigated by measuring the zero order transmission through sandwiches made of the array and the desired materials. Four different interfaces were characterized including air-array-air, polyethylene-array-polyethylene, quartz-array-quartz, and silicon-array-silicon[21]. The quartz and polyethylene are fused quartz and low-density polyethylene, respectively. The surrounding silicon was moderately n-doped with a resistivity of 20 Ω cm. These surrounding media were fairly transparent to terahertz radiation and have different refractive indices of 1, 1.51, 1.98 and 3.42, respectively, for Air, polyethylene, quartz and silicon. The same subwavelength-structured sample was used as the array and the resonance peaks in the transmission spectra were confirmed by placing the major axis of the hole perpendicular to the terahertz polarization ($E||x$). The amplitude transmission spectra for different interfaces are shown in Fig. 8(b), where the [±1,0] modes are represented by the dashed lines. The experimental result revealed that with increasing refractive index of the surrounding dielectric media, the peak amplitude decreases while the corresponding resonance peak moves toward the lower frequencies as predicted by Equation (1). This result is also consistent with the experimental observation in the optical region[32]. The observed resonant frequencies of the [±1, 0] mode as a function of the surrounding refractive index is plotted in the inset of Fig. 8(b). The low-index material clearly showed pronounced maxima and minima due to the resonant excitation of SPs and Wood's anomaly, respectively. For high-index material, however, the pronounced maxima were relatively broader because of the merging of consecutive resonance peaks. The Wood's anomaly effect also appeared to be weaker due to overlapping with the resonance peaks.

5.2 Transition of a SP resonance from a photonic crystal effect

So far we have demonstrated the static hole arrays whose dielectric constant remain fixed. It is thus intriguing to observe, how the SP resonance can be evolutionally developed when the real part of dielectric function of the constituent medium is altered instantaneously from positive, across zero to negative? In an effort to investigate such a question, we observed a characteristic evolution of a SP resonance in a semiconductor subwavelength hole array by use of optical pump-terahertz probe measurements[23].

The array sample was made from lightly n-doped ($4\times10^{14}\,cm^{-3}$) silicon (30-μm-thick), a fairly transparent medium to terahertz radiation. Its relatively low carrier density is insufficient to support SP resonances. The experimental result revealed that the terahertz transmission properties of the unexcited array at room temperature were dominated by the out-of-plane two-dimensional photonic crystal effect[33]. When optical excitation was applied to the array, the photo-generated free carriers altered the dielectric properties of Si; the real part of dielectric constant changed from positive to negative with increasing excitation intensity. As a result, the signature of photonic crystal effect gradually disappeared and SP resonance emerged and was developed into extraordinary terahertz transmission.

Figure 9(a) illustrates the transmitted terahertz pulses through air reference, blank Si, and the array of both perpendicular and parallel orientations before and after the optical excitation of a 111-mW average power. The perpendicular (parallel) orientation of the array is defined with the longer axis of the elliptical hole perpendicular (parallel) to terahertz electric field. The transmitted terahertz pulse through the unexcited blank Si showed a ~85% amplitude transmission if surface reflections are taken into account. The Si became nearly opaque to terahertz radiation under intense optical excitation due to strong absorption by the photo-generated free carriers. The corresponding Fourier-transformed spectra are shown in Fig. 9(b). In the absence of optical excitation the array can be considered as a two-dimensional out-of-plane photonic crystal slab that has shown complicated spectral structures instead of stopgaps[33]. Under intense optical excitation, however, the transmission spectra exhibited totally different features; the photonic crystal resonances disappeared and SP resonance peaks occured at different frequencies.

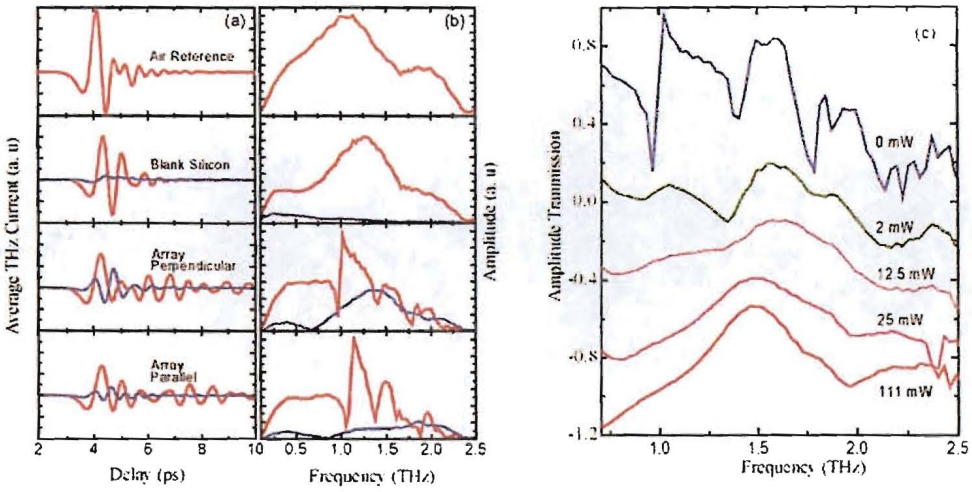

Fig. 9. Transmitted THz pulses through air, blank Si substrate and the gratings are shown in (a) and the corresponding spectra are shown in (b). The red curves represent unexcited samples and the blue curves represent the photoexcited samples. (c) is the measured amplitude transmission through the grating as a function of the pump power. The spectra are vertically displaced for clarity.

The metallic behavior of the array is mainly determined by the negative value of the real dielectric constant $\varepsilon_{rm} < 0$. Under intense optical excitation, the Si array became a complex multilayer medium, composing of a stack of photo-excited Si and unexcited Si layers. At terahertz frequencies, ε_{rm} of the photo-excited layer may turn to negative from being positive under appropriate laser excitation and hence the sample behaved as a metallic array that favored the formation of SPs. The thickness of the photo-excited layer depends on the penetration depth δ_L at the excitation laser wavelength, here $\delta_L = 10\,\mu\text{m}$ for Si at $\lambda = 800\,\text{nm}$[34]. In contrast, the penetration depth for terahertz radiation in the photo-excited Si is $\delta_{THz} = 3.69\,\mu\text{m}$ at 1.50 THz under 111-mW excitation[4], corresponding to an carrier density $N = 0.99 \times 10^{18}\,\text{cm}^{-3}$. δ_{THz} can be influenced by laser intensity and it became thinner with increasing optical excitation.

The frequency-dependent terahertz amplitude transmission of the array under optical excitation is plotted in Fig. 9(c). Transmission is found to be dominated by the SPP resonances at optical excitation power of 111 mW. We observed a strong resonance at 1.50 THz due to the fundamental SP [±1, 0] THz mode for perpendicular orientation which is accompanied by a transmission minimum occurred at 1.95 THz due to the Wood's anomaly[21]. Figure 9(c) also depicted the characteristic evolution of the photo-induced SP resonance, the laser excitation was varied from 0 to 111 mW. We observed that the real dielectric constant ε_{rm} was evolutionally tuned from positive, across zero to negative with increasing optical excitation power. Above 3 mW, the photo-excited Si layer began to exhibit metallic properties and had a potential to support SPs. At low excitation, the transmission was dominated by complex out-of-plane photonic crystal resonances near 0.97, 1.40, and 1.78 THz. When the laser power was increased to 12.5 mW, the photonic crystal effect nearly disappeared; a new resonance peak occurs at 1.60 THz due to the excitation of SPs. The further increase in excitation power gave rise to an enhanced terahertz transmission and a red-shift of resonance peak to 1.50 THz. The transmission efficiency at the SP resonance 1.50 THz was found to increase with increasing power of laser excitation. At 25 mW of optical excitation power, the resonance peak terahertz transmittance was 25.5%, and peak was increased to 45% at 111-mW of optical excitation power.

6 SPP switching

Highly frequency selective resonance properties have potential to be used in THz devices such as active filters, modulators, and switches. In this section, we present the control of the SPP resonances using electrical and optical

techniques. In both cases, the applied electric and optical fields modify the dielectric properties of the substrate materials and hence control the resonance peak. The optical technique can be operated at ultrafast time scale by incorporate a substrate having ultrafast photo-responses.

6.1 Electrical Switching of SP Resonances

In this section, we present electronically switchable surface plasmons resonance and extraordinary light transmission in the terahertz frequency range through metallic hole arrays fabricated on doped semiconductor substrates[35]. The hybrid metal-semiconductor forms a Schottky diode structure, where the depletion region can be actively modified in real-time by applying an external voltage bias. In this way we accomplish effective switching of the surface plasmons resonance enhanced THz transmission with an efficiency as high as 31% in amplitude (or 53% in intensity). The demonstration can be translated to other optical frequencies and provides a host of opportunities in the design and construction of future plasmonic devices.

In Figure 10(a-c) we show the conceptual design of the sub-wavelength metallic hole array for all-electronically switchable surface plasmon resonance. The slightly n-doped GaAS and the metallic film form a Schottky diode structure, where the depletion region can be actively controlled with an external voltage bias, thereby switching the damping of the SP resonance and the extraordinary THz transmission. The SP samples characterized here were fabricated on gallium arsenide (GaAs) substrate. The substrate has a 1-μm-thick n-doped GaAs layer with free carrier density of 3×10^{16} cm^{-3} deposited on an intrinsic GaAs wafer by molecular beam epitaxy (MBE). An ohmic contact surrounding but separating from the hole array region about 1~mm was fabricated by electron beam deposition of 20~nm of germanium, 20~nm of gold, 20~nm of nickel, and 200~nm of gold in sequence, then perform rapid thermal annealing at 400°C for 1 minute. The metallic hole array was fabricated using standard photolithographic methods and electron beam deposition of 10~nm of titanium and 200~nm of gold, then undertaking a lift-off process.

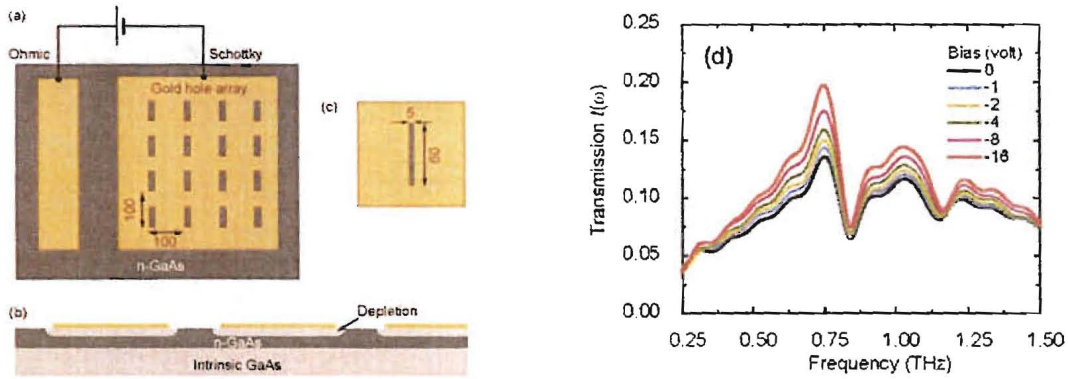

Fig. 10 Schematic design of all electronically switchable surface plasmon resonance. (b) Cross-sectional view of the structures to show the depletion region upon reverse voltage bias. (c) shows the hole geometries with dimensions in microns. (d) amplitude transmission of the THz electric field as a function of the applied reverse bias voltage.

The substrate charge carrier density and conductivity near the metal-substrate interface can be electronically modified upon a reverse voltage due to the formation of the Schottky diode structure. Higher the reverse voltage bias increases the depletion thereby reducing the damping of SP resonance. Fig. 10(d) shows the experimental results. We observed increasing THz transmission at the peaks as the applied reverse voltage bias increases, while the transmission dips (Wood's anormalies) are much less affected. Due to the evanescent nature, SP resonance is extremely sensitive to the material properties in the vicinity of the metal interface. In case of no voltage bias, the conducting substrate results in a large loss as well as a "short-circuit" of the metallic holes, thereby damping the SP resonance. Upon a reverse voltage bias, the increasing depletion reduces the substrate loss, thereby recovering the SP resonance and extraordinary THz transmission.

6.2 Ultrafast Optical Switching of SP Resonances

Here, we demonstrate ultrafast optical control of surface plasmon assisted terahertz (THz) transmission in a subwavelength metallic hole array on a ErAs:GaAs superlattice substrate. The transient photoconductivity of the substrate allows modulation of the THz resonance amplitude via optical excitation with a time scale of ~10 ps. ErAs:GaAs superlattices have already proven to benefit many ultrafast applications such as THz photoconductive receivers, fast switchable THz metamaterials[36], etc. They have the unique property of having variable carrier lifetimes from hundreds of femtosecond to tens of picosecond by changing the supeerlattice period.

The 2D metallic gratings used for this work are fabricated on a 2-μm-thick ErAs:GaAs superlattice, formed by alternating layers of GaAs and ErAs nanoislands on a GaAs substrate[36], has a carrier lifetime of 8 picoseconds. Standard photolithography was used to fabricate the aluminum (200-nm-thick) hole arrays on ErAs:GaAs substrates. The holes are patterned in a square array with lattice constants of 100 μm and a rectangular hole dimension of 50 μm × 25 μm. The THz time domain spectrometer (THz TDS) used in this experiment utilizes a 1 kHz regeneratively amplified Ti:Sapphire laser capable of generating 3.2 mJ, 50 fs pulses at 800 nm. Part of the output laser power is used for THz generation and detection using ZnTe crystals via optical rectification and the electro-optic effect. The remainder of the optical power passes through a variable attenuator to form a ~10 mm diameter illumination spot at the sample at an angle of ~10°. Figure 11(a) shows transmitted THz radiation ($T(\omega)=|E_{tr}(\omega)/E_{in}(\omega)|$) through the ErAs:GaAs grating when normalized by the transmission of a blank GaAs reference slab. The resonance frequency of the fundamental SPPs' mode of such 2D grating at normal incidence is approximately given by $f_{res}=c/(L\sqrt{\varepsilon_s})$, where L is the grating's period, and ε_s is the dielectric constant of the substrate.

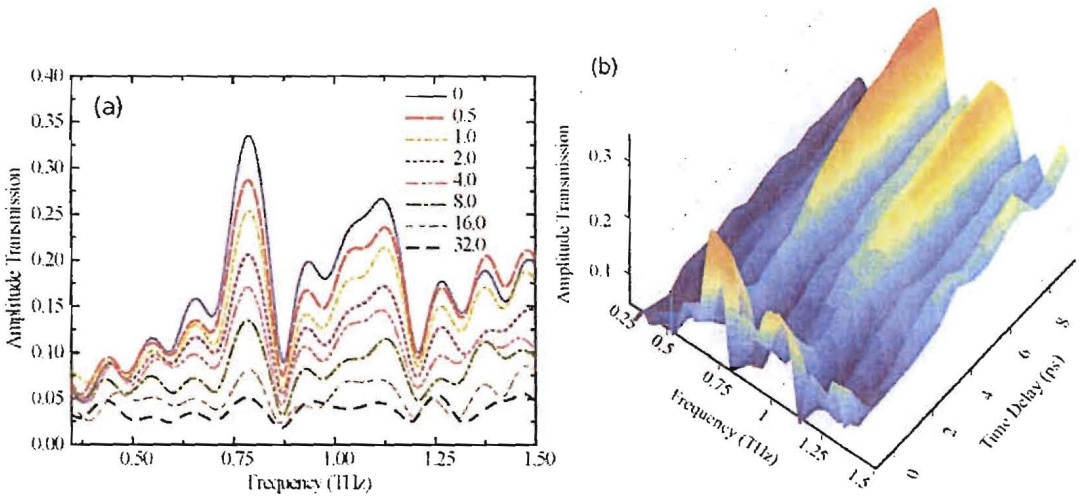

Fig. 11(a) Resonant THz transmission spectra through a 2D metallic grating on a ErAs:GaAs superlattice substrate. Pump fluence (μJ/cm^2) dependence of the transmission is represented by different colors. Fig. 2(b) shows pump delay dependent transmission spectra with an optical fluence of 8 μJ/cm^2.

The photo-generated carriers create a conductive path in the substrate which resists the scattering and coupling of the SPPs at hole edges. The resonance amplitude reduces monotonically as the pump fluence increases. At higher fluences the substrate becomes metallic and the THz transmission through the grating suffers higher attenuation. The resonance peak frequencies remain unchanged under the optical excitation. We obtained almost 70% modulation depth with a pump fluence of 8 μJ/cm^2. Resonance amplitudes keep reducing with increasing fluences until we observe a complete switch-off of the transmitted THz resonance for an optical fluence of ~32 μJ/cm^2. The photoexcited layer of the substrate forms conducting paths in the hole areas and the holes behave as "short circuit" which eventually resists scattering of the SP electromagnetic waves. Also, the bulk photoexcited substrate behaves as a Drude metal and attenuates the direct transmission through the holes at higher fluences. Figure 11(b) shows resonance THz transmissions as a function of the delays of the 8 μJ/cm^2 optical pump. Measurements clearly reveal the annihilation and formation of the resonance transmission at 0.8 THz. Transmission shows a strong resonance before arrival of the optical pulses, which

then undergoes strong attenuation, and eventually recovers as the time delay increases. The resonance recovery time is ~10 ps which is consistent with the measured carrier lifetime of the substrate.

6 Conclusion

We studied transmission properties of terahertz radiation in 2D plasmonic array of subwavelength holes using THz-TDS. The plasmonic samples were fabricated using conventional photolithography. The frequency-dependent resonant transmission in the 2D hole arrays is understood as a consequence of the resonance excitation of SPs at the metal-dielectric interface. We demonstrated the effect of hole shape, hole dimensions, dielectric properties of the metals, polarization dependence, and metal thickness on enhanced terahertz transmission. Rectangular hole shapes were found to show higher resonant transmission when the polarization of the incident terahertz field is perpendicular to the longer axis of the holes. Efficiently enhanced transmission was also observed in optically thin metallic arrays having thickness of one-third of the skin depth. For similar array transmission is higher for the array made from metal having higher electrical conductivity. Enhanced terahertz transmission was demonstrated in plasmonic arrays made from doped semiconductors that possess negative values of the real part of dielectric function. We also demonstrated the SP resonances in photoexcited semiconductor and tuning the resonance amplitude by varying the optical excitation power. In addition, both electrical and optical techniques have been demonstrated for efficient control of the Surface Plasmon resonances in 2D plasmonic arrays.

Acknowledgement

The authors thank J. Han, D. Qu, D. Grischkowsky, Y. Zhao, X. Lu, J. Dai, J. Xu, J. Chen, X.-C. Zhang, M. He, and M. Gong for their outstanding contributions and efforts in this work. This work was performed in part, at the Center for Integrated Nanotechnologies, a U. S. Department of Energy, Office of Basic Energy Sciences nanoscale science research center jointly operated by Los Alamos and Sandia National Laboratories. Los Alamos National Laboratory, an affirmative action equal opportunity employer, is operated by Los Alamos National Security, LLC, for the National Nuclear Security Administration of the U. S. Department of Energy under contract DE-AC52-06NA25396.The authors from Oklahoma State University gratefully acknowledge the support of the U.S. National Science Foundation.

References

1. T. W. Ebbesen, H. J. Lezec, H. F. Ghaemi, T. Thio, and P. A. Wolff, Nature **391**, 667 (1998).
2. W. L. Barnes, A. Dereux, and T. W. Ebbesen, Nature **424**, 824 (2003).
3. R. Gordon, A. G. Brolo, A. McKinnon, A. Rajora, B. Leathem, and K. L. Kavanagh, Phys. Rev. Lett. **92**, 037401 (2004).
4. H. Raether, *Surface plasmons on smooth and rough surfaces and on gratings* (Springer-Verlag, Berlin, 1988), Chap. 2, p. 4.
5. E. Ozbay, Science **311**, 189 (2006).
6. D. Qu, D. Grischkowsky, and W. Zhang, Opt. Lett. **29**, 896 (2004).
7. C. Janke, J. G. Rivas, C. Schotsch, L. Beckmann, P. H. Bolivar, and H. Kurz, Phys. Rev. B **69**, 205314 (2004).
8. H. Cao and A. Nahata, Opt. Express **12**, 1004 (2007).
9. F. Miyamaru and M. Hangyo, Appl. Phys. Lett. **84**, 2742 (2004).
10. J. O'Hara, R. D. Averitt, and A. J. Taylor, Opt. Express **12**, 6397 (2004).
11. D. Qu and D. Grischkowsky, Phys. Rev. Lett. **93**, 196804 (2004).
12. J. B. Masson and G. Gallot, Phys. Rev. B **73**, 121401 (2006).
13. A. Agrawal, T. Matsui, Z. V. Vardeny, and A. Nahata, J. Opt. Soc. Am B **24**, 2545 (2007).
14. T. Thio, H. F. Ghaemi, H. J. Lezec, P. A. Wolff, and T. W. Ebbesen, J. Opt. Soc. Am B **16**, 1743 (1999).
15. D. E. Grupp, H. J. Lezec, T. W. Ebbesen, K. M. Pellerin, and T. Thio, Appl. Phys. Lett. **77**, 1569 (2000).
16. M. A. Ordal, L. L. Long, R. J. Bell, S. E. Bell, R. R. Bell, R. W. Alexander, Jr., and C. A. Ward, Appl. Opt. **22**, 1099 (1983).
17. L. Martín-Moreno, F. J. García-Vidal, H. J. Lezec, A. Degiron, and T. W. Ebbesen, Phys. Rev. Lett. **90**, 167401 (2003).
18. A. K. Azad and W. Zhang, Opt. Lett. **30**, 2945 (2005).
19. A. K. Azad, M. He, Y. Zhao, and W. Zhang, Opt. Lett. **31**, 2637 (2006).
20. J. Gómez Rivas, C. Schotsch, P. Haring Bolivar, and H. Kurz, Phys. Rev. B **68**, 201306 (2003).

21. A. K. Azad, Y. Zhao, and W. Zhang, Appl. Phys. Lett. **86**, 141102 (2005).
22. J. G. Rivas, C. Janke, P. Bolivar, and H. Kurz Opt. Express **13**, 847 (2005).
23. W. Zhang, A. K. Azad, J. Han, J. Xu, J. Chen, and X.-C. Zhang, Phys. Rev. Lett. **98**, 183901 (2007).
24. E. Hendry, F. J. Garcia-Vidal, L. Martin-Moreno, J. G. Rivas, M. Bonn, A. P. Hibbins, and M. J. Lockyear, Phys. Rev. Lett. **100**, 123901 (2008).
25. B. Ferguson and X.-C. Zhang, Nature Materials **1**, 26 (2002).
26. J. Han, A. K. Azad, M. Gong, X. Lu, and W. Zhang, Appl. Phys. Lett. **91**, 071122 (2007).
27. V. M. Agranovich, and D. L. Mills, *Surface Polaritons* (North-Holland, New York, 1982).
28. K. Molen, K. Koerkamp, S. Enoch, F. Segerink, N. Kulst, and L. Kuipers, Phys. Rev. B **72**, 045421 (2005).
29. Z. Ruan and M. Qiu, Phys. Rev. Lett. **96**, 233901 (2006).
30. W. Fan, S. Zhang, B. Minhas, K. J. Malloy, and S. R. J. Brueck, Phys. Rev. Lett. **94**, 033902 (2005).
31. R. W. Wood, Phys. Rev. **48**, 928 (1935).
32. T. Kim, T. Thio, T. Ebbesen, D. Grupp, and H. Lezec, Opt. Lett. **24**, 256 (1999).
33. Z. Jian and D. Mittleman, Appl. Phys. Lett. **87**, 191113 (2005).
34. H. F. Ghaemi, T. Thio, D. E. Grupp, T. W. Ebbesen, H. J. Lezec, Phys. Rev. B **58**, 6779 (1998).
35. H. –T. Chen, H. Lu, A. K. Azad, R. D. Averitt, A. C. Gossard, S. A. Trugman, J. F. O'Hara, and A. J. Taylor, Opt. Express **16**, 7641 (2008).
36. R. P. Prasankumar, A. Scopatz, D. J. Hilton, A. J. Taylor, and R. D. Averitt, Appl. Phys. Lett. **86**, 201107 (2005).

Filename:	SPP_Rev120208.doc
Directory:	E:\Azad\Photonic West
Template:	E:\Documents and Settings\azad\Application Data\Microsoft\Templates\Normal.dot
Title:	Terahertz spectroscopy of two-dimensional subwavelength
Subject:	
Author:	A Azad
Keywords:	
Comments:	
Creation Date:	12/2/2008 3:34:00 PM
Change Number:	2
Last Saved On:	12/2/2008 3:34:00 PM
Last Saved By:	azad
Total Editing Time:	7 Minutes
Last Printed On:	2/3/2009 5:09:00 PM
As of Last Complete Printing	
Number of Pages:	15
Number of Words:	8,376 (approx.)
Number of Characters:	46,490 (approx.)